PCCP

Physical Chemistry Chemical Physics

www.rsc.org/pccp

Volume 11 | Number 44 | 28 November 2009 | Pages 10229–10528

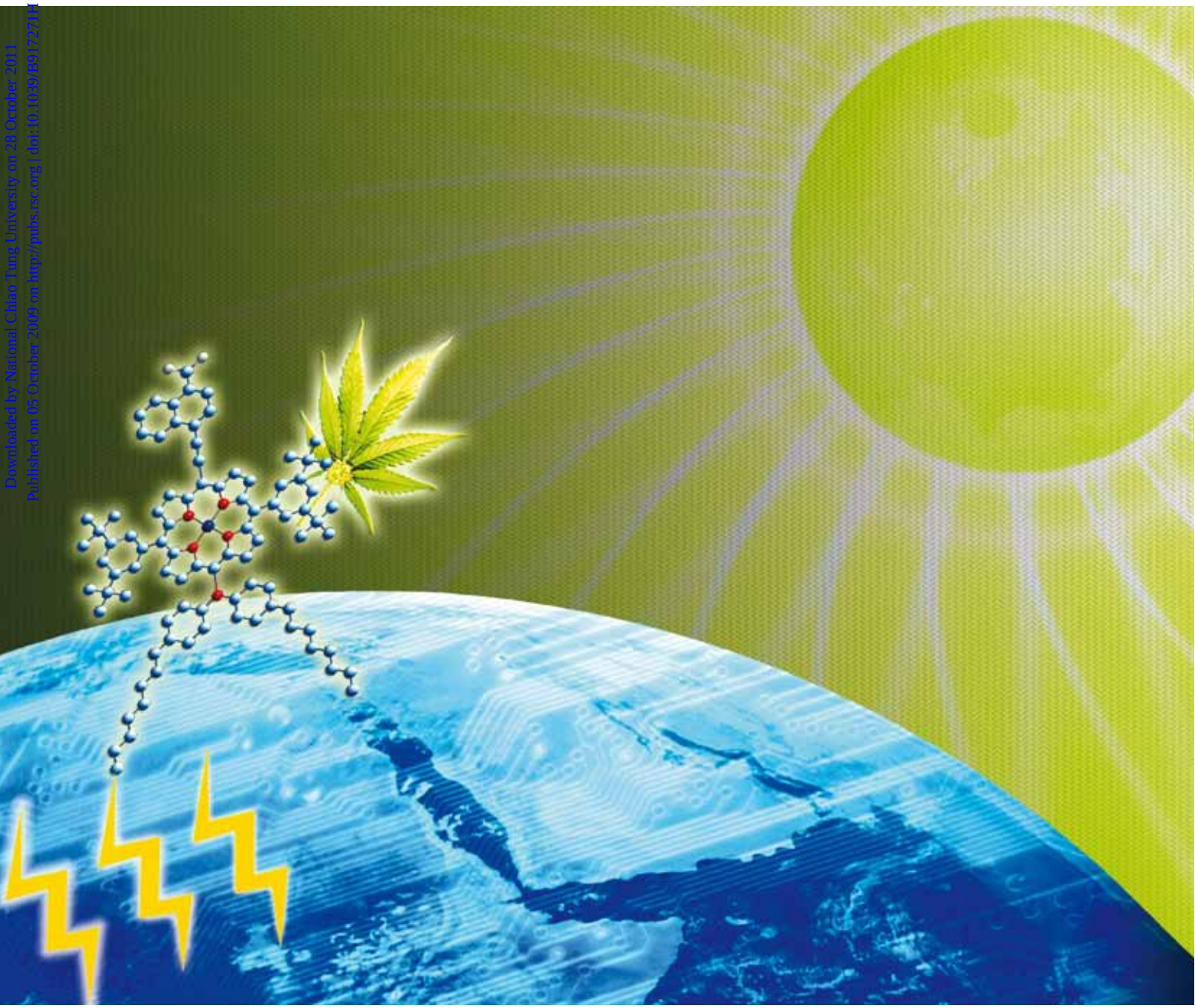

ISSN 1463-9076

Design and characterization of highly efficient porphyrin sensitizers for green see-through dye-sensitized solar cells†

Hsueh-Pei Lu,[a] Chi-Lun Mai,[b] Chen-Yuan Tsia,[a] Shun-Ju Hsu,[a] Chou-Pou Hsieh,[b] Chien-Lan Chiu,[b] Chen-Yu Yeh*[b] and Eric Wei-Guang Diau*[a]

Received 22nd August 2009, Accepted 23rd September 2009
First published as an Advance Article on the web 5th October 2009
DOI: 10.1039/b917271h

YD12 (η = 6.7%) is a green sensitizer remarkable for its outstanding cell performance beyond that of N719 (η = 6.1%) with no added scattering layer; the additional scattering layer assists N719 in promoting the efficiency in the red shoulder of the spectrum, but has only a small effect on the improvement of the cell performance for porphyrins.

As a cost-effective energy-conversion device, dye-sensitized solar cells (DSSC) have received much attention after the pioneering work of Grätzel and co-workers.[1] These devices with Ru complexes as photosensitizers have attained the greatest efficiency ($\eta \sim 11\%$) of conversion of photovoltaic power,[2] but the limited availability of Ru dyes and their environmental concerns have stimulated much effort to find cheaper and safer alternative organic-based dyes.[3] Among those non-Ru-based dyes, porphyrin chromophores are promising candidates because of their efficient capture of solar energy in the visible region. Numerous reports on porphyrin-based DSSC have appeared.[4] In principle, the molecular design of a porphyrin sensitizer is based on a **P–B–A** structure, in which **B** represents a π-conjugation bridge serving as a spacer between the porphyrin light-harvesting center **P** and the carboxyl anchoring group **A**. A DSSC device using porphyrin sensitizers with the **B–A** unit functionalized at the β-position is reported to have attained a cell performance as great as η = 7.1%;[4d] the *meso*-substituted porphyrins gave smaller η values.[4f,g,i,j] The effects of porphyrin aggregation on the TiO_2 surface,[4e,5] the bridge length of the sensitizers,[5c,6] and the position and the number of the **B–A** units[4e,j,6a] have all been investigated to rationalize the performance of the cell. We have reported a novel zinc porphyrin dye (**YD1**) with a molecular design based on a concept of a **D–P–B–A** structure (Scheme 1), simply adding an electron-donating diarylamino group (**D**) attached at the *meso*-position of **P** opposite the *meso*-substituted phenylethynylcarboxyl anchoring group.[7] A device made from this porphyrin dye has a cell performance similar to that of a Ru-based DSSC, making the push-pull porphyrin the most efficient green dye for DSSC applications.[7]

Here we report the cell performance for three new porphyrin sensitizers (**YD11–YD13**, Scheme 2): **YD11** was modified from **YD1** for which the two *tert*-butyl groups in the diarylamino substituent were replaced by two hydrocarbon long chains to improve its thermal and photochemical stability in a device. This design mimics the strategy applied in an amphiphilic ruthenium polypyridyl sensitizer (**Z907**) that has shown excellent stability toward water-induced desorption under both thermal stress and light-soaking conditions.[8] **YD12** and **YD13** have the same diarylamino substituent as in **YD11** but with the phenyl group in **B** being replaced by naphthalene and anthracene, respectively. Fig. 1 shows the absorption spectra of **YD11–YD13** in ethanol solution; the Soret and Q bands shift toward longer wavelengths as the π system in **B** is expanded, because of the spectral coupling between the aromatic substituent and the porphyrin ring. This coupling effect was exceptionally pronounced in **YD13**, for which both Soret and Q bands become significantly broad and red-shifted. We investigated the electrochemical properties of these porphyrins using cyclic voltammetry. The measured oxidation and reduction potentials of **YD11–YD13** are summarized in Table S1;† the corresponding energy-level diagram showing the HOMO and the LUMO of each porphyrin is depicted in Fig. S1.† These results indicate that electron injection from the LUMO of the excited porphyrin to the conduction band of TiO_2 and dye regeneration from redox couple I^-/I_3^- to the HOMO of the porphyrin cation are feasible.

Because of the large absorption coefficients of these porphyrins, we expect that thinner TiO_2 films might suffice to produce a reasonable cell performance. We accordingly prepared three TiO_2/FTO working electrodes with TiO_2 film thicknesses (L) ~5, ~10 and ~(10 + 4) μm for photovoltaic

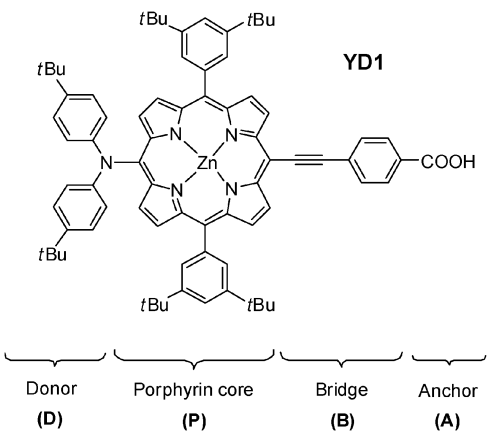

Scheme 1 Molecular design of **YD1** based on a **D–P–B–A** structure.

[a] *Department of Applied Chemistry, National Chiao Tung University, Hsinchu 300, Taiwan. E-mail: diau@mail.nctu.edu.tw*
[b] *Department of Chemistry, National Chung Hsing University, Taichung 402, Taiwan. E-mail: cyyeh@dragon.nchu.edu.tw*

† Electronic supplementary information (ESI) available: The details of synthetic procedures, electrode preparation and device fabrication, dye-loading examination, photovoltaic characterization, femtosecond fluorescence spectroscopy, and supplementary tables (Table S1–S5) and figures (Fig. S1–S5). See DOI: 10.1039/b917271h

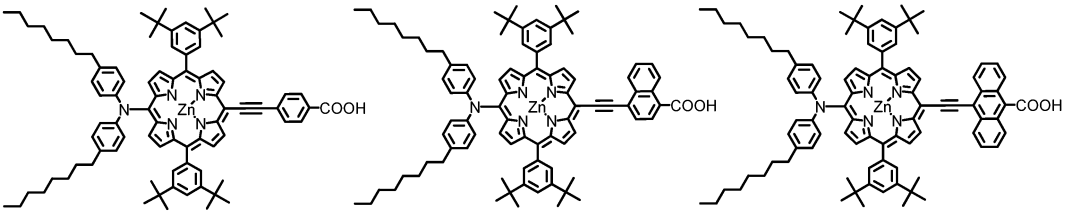

Scheme 2 Structures of **YD11–YD13**.

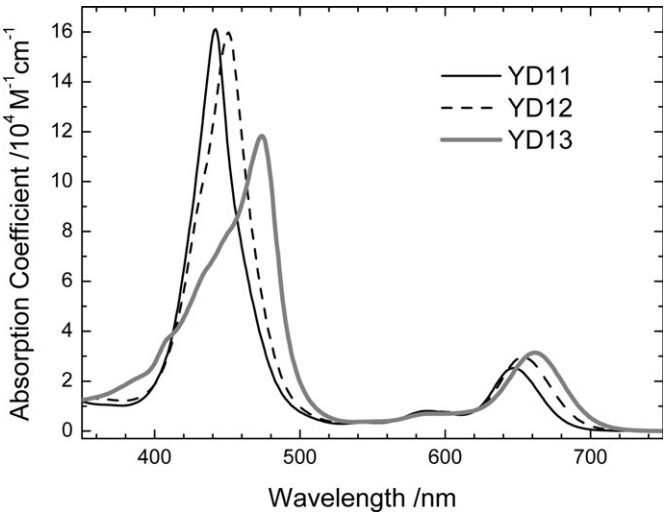

Fig. 1 Calibrated absorption spectra of **YD11–YD13** in ethanol.

measurements (the corresponding SEM images are shown in Fig. S2†). As the first two TiO_2 films (A and B) contain only the active layer (particle size ~20 nm), the films were essentially transparent before dye loading and they can be see-through after dye loading. The third TiO_2 film (C) has the same active layer as the second one (~10 μm) but with an additional scattering layer (~4 μm, particle size 200–600 nm) to improve further the light-harvesting efficiency. The corresponding DSSC devices were fabricated according to a standard procedure reported elsewhere.[6b,7,9]

The photovoltaic measurements were performed with three to four identical working electrodes for each porphyrin (**YD11–YD13**) adsorbed on each TiO_2 film (A–C) under the same experimental conditions. The raw data from each *J–V* measurement are summarized in Tables S2–S4† for films A–C, respectively; the corresponding averaged photovoltaic parameters are summarized in Table 1. Fig. 2a–c show one set of typical *J–V* curves (working electrode "a" in Tables S2–S4†) of the porphyrin-based DSSC devices for TiO_2 films A–C, respectively; for comparison, the cell performances of the devices made of N719 dye with the same TiO_2 films as for **YD11–YD13** are shown as dashed curves in each plot. Our results indicate that both **YD11** and **YD12** exhibit exceptionally superior performance relative to N719 dye; the poor performance of **YD13** is remarkable and is discussed below. The short-circuit photocurrent densities (J_{SC}) of the two promising porphyrin-based devices are significantly greater than those of the **N719** devices, in particular for those of film B (Fig. 2b). Even though the open-circuit photovoltages (V_{OC}) and fill factors (FF) for the former are smaller than for the latter, the net effects of these variations make the overall efficiencies of power conversion of the **YD11** and **YD12** devices outperform those of the **N719** devices at $L \sim 10$ μm without a scattering layer (Fig. 2b). **YD11** ($\eta = 6.6\%$) and **YD12** ($\eta = 6.7\%$) are thus two remarkable green sensitizers for their outstanding cell performances relative to that of **N719** ($\eta = 6.1\%$) without an added scattering layer (film B) for light-penetrable DSSC applications. When the ~10-μm TiO_2 films were covered with a scattering layer (film C), we found that the cell performance of **N719** was significantly improved to $\eta = 7.3\%$ whereas the performances of the porphyrin dyes increased only slightly ($\eta = 6.8\%$ and 7.0% for **YD11** and **YD12**, respectively, Fig. 2c). Our results indicate that a substantial increase in J_{SC} for the **N719** device is a key factor for the improvement of the cell performance with the addition of a scattering layer. To understand why the scattering layer was insensitive to the cell performances of the porphyrin-based devices, we performed measurements of the incident photon-to-current conversion efficiency (IPCE) for each device.[10]

Fig. 3a–c show the efficiency spectra of the same DSSC devices of which the corresponding *J–V* characteristics are shown in Fig. 2a–c. Integrating the IPCE over the AM 1.5G solar spectrum gives a calculated J_{SC} similar to the collected value for all devices under investigation (Fig. S3†). There are three important points deduced from our IPCE results. First, the efficiency spectra of both **YD11** and **YD12** sensitizers are similar for all three TiO_2 films, but the spectra of **YD12** have a Q-band shoulder slightly extended to longer wavelengths, which increases slightly J_{SC} for **YD12** relative to **YD11**. This

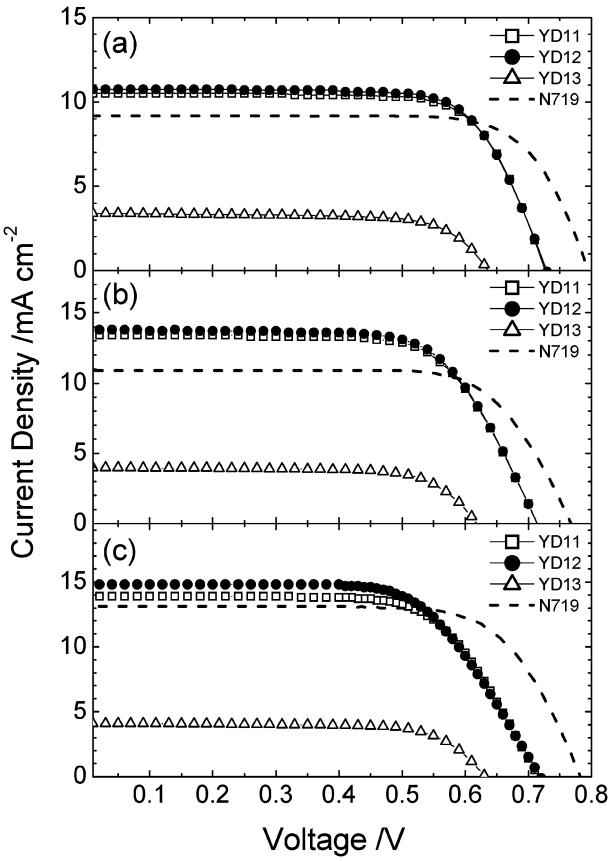

Fig. 2 Current–voltage characteristics of DSSC devices (working electrode "a" in ESI†) with sensitizers of **YD11–YD13** as indicated (open squares: **YD11**; filled circles: **YD12**; open triangles: **YD13**) under illumination of simulated AM1.5 full sunlight (100 mW cm^{-2}) with an active area 0.16 cm^2 of three film thicknesses: (a) ~5 μm (film A); (b) ~10 μm (film B); (c) ~(10 + 4) μm (film C). The dashed curves show the results of the **N719** devices for comparison.

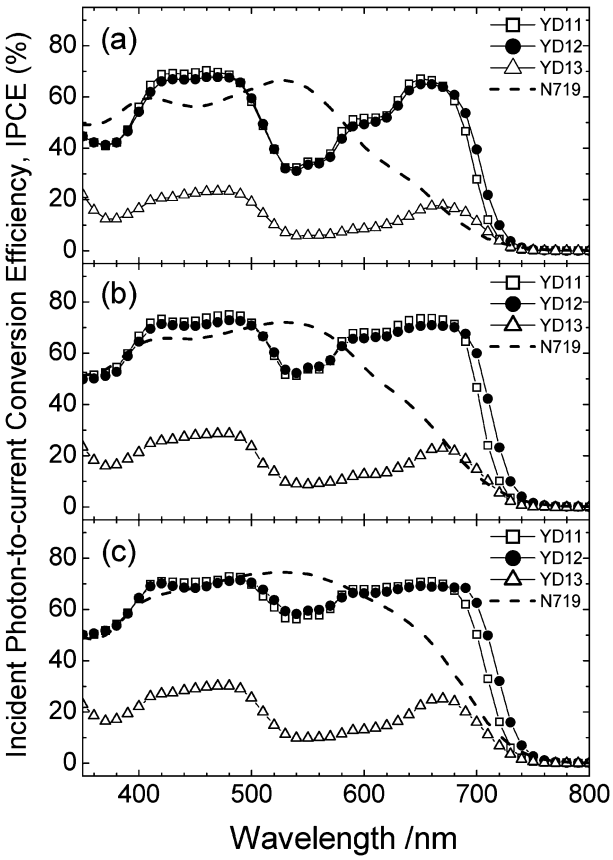

Fig. 3 Corresponding IPCE action spectra of the same DSSC devices as those shown in Fig. 2. The dashed curves show the results of the **N719** devices for comparison.

effect is consistent with the absorption spectral feature shown in Fig. 1. Second, the efficiency spectra of **YD13** show smaller values than those of **YD11** and **YD12**, which explains its poor performance. This effect is inconsistent with the absorption feature shown in Fig. 1 and is discussed in the next section. Third, the efficiency spectra of **YD11** and **YD12** involve a large gap between the Soret and the Q bands in film A (Fig. 3a), but this gap became smaller when thicker TiO_2 films (B) were applied (Fig. 3b). On addition of another scattering layer (film C), the gaps in **YD11** and **YD12** became even smaller

Table 1 Photovoltaic parameters of DSSC with photosensitizers **YD11–YD13** and **N719** as a function of TiO_2 film thickness (L) under simulated AM-1.5 illumination (power 100 mW cm^{-2}) and active area 0.16 cm^{2a}

L/μm	Dye	Dye-loading/nmol cm^{-2}	J_{SC}/mA cm^{-2}	V_{OC}/V	FF	η/%
~5	**YD11**	75	10.54 ± 0.33	0.723 ± 0.013	0.73 ± 0.01	5.54 ± 0.11
(Film A)	**YD12**	82	10.75 ± 0.34	0.724 ± 0.009	0.72 ± 0.02	5.60 ± 0.09
	YD13	62	3.30 ± 0.16	0.633 ± 0.006	0.71 ± 0.01	1.49 ± 0.08
	N719	90	9.27 ± 0.13	0.794 ± 0.006	0.74 ± 0.01	5.47 ± 0.03
~10	**YD11**	154	12.99 ± 0.83	0.715 ± 0.006	0.71 ± 0.03	6.56 ± 0.09
(Film B)	**YD12**	160	13.77 ± 0.40	0.714 ± 0.005	0.68 ± 0.02	6.69 ± 0.09
	YD13	129	3.97 ± 0.10	0.618 ± 0.002	0.72 ± 0.01	1.76 ± 0.04
	N719	178	10.97 ± 0.42	0.769 ± 0.002	0.73 ± 0.02	6.16 ± 0.14
~(10 + 4)	**YD11**	[b]	14.01 ± 0.14	0.716 ± 0.003	0.68 ± 0.01	6.79 ± 0.12
(Film C)	**YD12**	[b]	14.23 ± 0.82	0.717 ± 0.008	0.68 ± 0.03	6.91 ± 0.15
	YD13	[b]	4.12 ± 0.08	0.630 ± 0.002	0.72 ± 0.01	1.86 ± 0.04
	N719	[b]	13.08 ± 0.31	0.786 ± 0.007	0.71 ± 0.01	7.27 ± 0.14

[a] The photovoltaic parameters are the averaged values obtained from analysis of the J–V curves of three-four identical working electrodes for each device fabricated and characterized under the same experimental conditions; the raw data of each J–V measurement are summarized in Tables S2–S4,† for films A–C, respectively; the uncertainties represent two standard deviations of the measurements. [b] The dye-loading amounts are similar to those of the corresponding films of the same thickness without a scattering layer (film B).

so that the efficiency spectra display a nearly flat nature in the entire visible region, 400–700 nm (Fig. 3c). The shoulders of the efficiency spectra on the red side extended no further beyond the edge of the Q band in the presence of a scattering layer; for this reason only a slight improvement in J_{SC} was found for the porphyrin-based DSSC with a scattering layer. In contrast, a significant improvement in cell performance was found for a **N719**-based DSSC with a scattering layer, because of the effective scattering effect in the red shoulder of the efficiency spectrum. Based on the above observations, we conclude that the involvement of the partially allowed triplet MLCT states of ruthenium complexes[2a] is responsible for the enhanced efficiency in the red shoulder of the IPCE spectrum of N719, whereas the effect of spin–orbit coupling in zinc porphyrins was insufficient for $S_0 \rightarrow T_1$ transitions to occur; the additional scattering layer thus provides no improvement of the efficiency spectra of **YD11–YD13** beyond the Q-band absorptions.

We applied femtosecond fluorescence decays to investigate the dynamics of interfacial electron injection in the porphyrin/TiO_2 films (film A), with porphyrin/Al_2O_3 films serving as references ($L \sim 5$ μm). The corresponding absorption spectra of the thin-film samples appear in Fig. S4.† An additional band at ~800 nm occurred for porphyrin-sensitized TiO_2 films (~820 nm for **YD13**), but this spectral feature was absent from all porphyrin-sensitized Al_2O_3 films. In our previous work on the spectroelectrochemistry of **YD1**, a characteristic band at ~800 nm was observed for the oxidized species of **YD1**.[7] The presence of such a band at ~800 nm for the **YD1**/TiO_2 film thus indicates the formation of species **YD1**$^+$; the same is true for all other porphyrin sensitizers (**YD11–YD13**) sensitized on TiO_2 films found here. For the sensitized Al_2O_3 films, the cationic spectral feature was absent because the excited electrons of the porphyrin sensitizers cannot inject into the conduction band of Al_2O_3 to form the cationic species on the Al_2O_3 surface.[11]

Femtosecond excitation of the thin-film samples was performed at 430 nm using a fluorescence up-conversion system described elsewhere.[5b] The emissions at the intensity maximum were optically gated with the fundamental pulse (860 nm) to yield the emission decays of **YD11–YD13**/TiO_2 films shown in Fig. 4a–c; those of **YD11–YD13**/Al_2O_3 films are shown for comparison. The temporal profiles of all samples show multi-exponential decay, and the corresponding time coefficients were obtained on analyzing the data with a parallel kinetic model.[5b,12] With the time coefficients weighted by their relative amplitudes (shown in parentheses), the average time coefficients of the TiO_2 films are determined to be all similar ($\tau_{TiO_2} \sim 1.8$ ps) for **YD11–YD13**; those of the Al_2O_3 films are determined to be $\tau_{Al_2O_3} = 10.8$, 10.6, and 4.8 ps, respectively. The emission decays of the Al_2O_3 films reflect only the intermolecular energy transfer due to aggregation of the dye on the Al_2O_3 surface, but the emission decays of the TiO_2 films contain not only the aggregate-induced energy transfer but also rapid electron injection from the excited state of a porphyrin into the conduction band of TiO_2. If we assume that the extent of dye aggregation on both TiO_2 and Al_2O_3 films is similar (Fig. S4†), based on the same amount of dye molecules adsorbed on the films, the quantum yields of **YD11**, **YD12** and **YD13** for electron injection on a TiO_2 surface become evaluated to be $\Phi_{inj} = 0.83$, 0.83 and 0.62, respectively.[13]

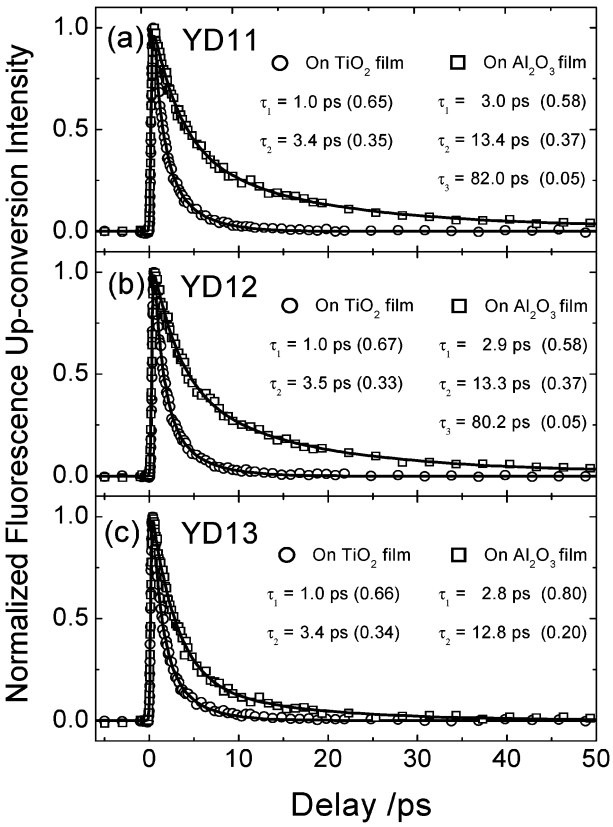

Fig. 4 Femtosecond emission decay curves of thin-film samples excited at the Soret band ($\lambda_{ex} = 430$ nm) and probed at the wavelength of maximum emission intensity. Panels (a)–(c) represent the transients of **YD11–YD13** on TiO_2 (circles) and on Al_2O_3 (squares) films. Solid curves represent theoretical fits with the corresponding time coefficients and relative amplitudes (in parentheses) as indicated.

In Fig. 4, the fluorescence decays are similar for all three porphyrins sensitized on TiO_2 films, but the fluorescence decay of **YD13** was much more rapid than that of **YD11** or **YD12** sensitized on Al_2O_3 films. Hence the presence of the anthracene group in the bridge from **YD13** to TiO_2 did not hamper the rate of interfacial electron transfer for the observed small injection yield. We consider two other possibilities responsible for the small injection yield of **YD13**: one is the anthracene-induced rapid intramolecular relaxation due to effective vibronic coupling, and the other is the anthracene-induced rapid relaxation of intermolecular energy due to aggregation. To examine the first possibility, we measured time-correlated single-photon counting (TCSPC) to determine the lifetimes of excited state of **YD11–YD13** in dilute solutions. All three porphyrins in ethanol (2×10^{-5} M) have similar lifetimes in a nanosecond range (1.3–1.4 ns). Ultrarapid non-radiative relaxation through intramolecular channel is thus excluded. For the other possibility, we performed photovoltaic measurements for **YD11–YD13** co-adsorbed with chenodeoxycholic acid (CDCA) on TiO_2 (film B) in a ratio [porphyrin]:[CDCA] = 1:2; the results appear in Fig. S5,† and the obtained photovoltaic parameters are summarized in Table S5.† The presence of CDCA slightly decreases J_{SC} for **YD11** and **YD12** through a slight reduction of the amount of dye loading, but CDCA plays a role to improve dye aggregation to some extent so as to significantly enhance the

J_{SC} for **YD13**. As a result, the efficiency of **YD13** greatly increased from 1.8% to 2.9% in the presence of CDCA. Anthracene thus induces much more rapid intermolecular energy transfer due to dye aggregation, leading to a cell performance for **YD13** poorer than for **YD11** and **YD12**.

The electron injection yield is an important factor to be considered to improve further the cell performance of the devices for organic dyes with a tendency to aggregate. For a Ru-based DSSC, in contrast, Φ_{inj} was expected to be $\sim$1.0,[1b,3b,14] but a smaller value ($\sim$0.9) was reported.[15] For porphyrin sensitizers such as **YD11** and **YD12**, even though several bulky *tert*-butyl groups and hydrophobic long alkyl chains were incorporated around the porphyrin macrocycle, the effect of aggregation cannot be completely eliminated: there is still room for improvement of porphyrin-based solar cells from the approach of the molecular design.

In summary, three push–pull zinc porphyrin sensitizers (**YD11–YD13**) were designed, synthesized and characterized for highly efficient green see-through photovoltaic applications. Both **YD11**- and **YD12**-sensitized solar cells exhibit excellent cell performances that outperform those of **N719**-based DSSC because of their exceptionally large photocurrents generated in the 400–700 nm region with no added scattering layer. The additional scattering layer assists **N719** in promoting the efficiency in the red shoulder of the spectrum, but has only a small effect on the improvement of cell performance for porphyrins. Moreover, the efficiency spectra of **YD12** have a Q-band shoulder slightly extended to longer wavelengths, which increases J_{SC} slightly and thus also increases η for **YD12** relative to **YD11**. With the addition of a scattering layer, the cell performance of **YD12** was comparable to that of **N719** (η = 6.91 $\pm$ 0.15% *vs.* 7.27 $\pm$ 0.14%). These porphyrins adsorbed on TiO_2 films have a long-lived cationic state occurring at $\sim$800 nm for its protracted charge recombination. Measurements of femtosecond fluorescence decay for all three porphyrins sensitized on TiO_2 and Al_2O_3 films determined the electron injection yields for **YD11**, **YD12**, and **YD13** to be 0.83, 0.83 and 0.62, respectively. The poor performance of **YD13** is understood to be due to the rapid aggregate-induced energy transfer in the presence of an anthracene group in the bridge. Work is in progress to diminish the effect of dye aggregation in the device, to improve its stability and to apply this series of porphyrin dyes for prospective applications in solid-state DSSC.[4d,16]

Acknowledgements

National Science Council of Taiwan and Ministry of Education of Taiwan, under the ATU program provided support for this project.

References

1 (*a*) B. O'Regan and M. Grätzel, *Nature*, 1991, **353**, 737; (*b*) M. K. Nazeeruddin, A. Kay, I. Rodicio, R. Humphry-Baker, E. Müller, P. Liska, N. Vlachopoulos and M. Grätzel, *J. Am. Chem. Soc.*, 1993, **115**, 6382; (*c*) M. Grätzel, *Inorg. Chem.*, 2005, **44**, 6841.

2 (*a*) M. K. Nazeeruddin, F. D. Angelis, S. Fantacci, A. Selloni, G. Viscardi, P. Liska, S. Ito, B. Takeru and M. Grätzel, *J. Am. Chem. Soc.*, 2005, **127**, 16835; (*b*) Y. Chiba, A. Islam, Y. Watanabe, R. Komiya, N. Koide and L. Han, *Jpn. J. Appl. Phys.*, 2006, **45**, L638; (*c*) F. Gao, Y. Wang, D. Shi, J. Zhang, M. Wang, X. Jing, R. Humphry-Baker, P. Wang, S. M. Zakeeruddin and M. Grätzel, *J. Am. Chem. Soc.*, 2008, **130**, 10720; (*d*) Y. Cao, Y. Bai, Q. Yu, Y. Cheng, S. Liu, D. Shi, F. Cao and P. Wang, *J. Phys. Chem. C*, 2009, **113**, 6290.

3 (*a*) N. Robertson, *Angew. Chem., Int. Ed.*, 2006, **45**, 2338; (*b*) T. W. Hamann, R. A. Jensen, A. B. F. Martinson, H. V. Ryswyk and J. T. Hupp, *Energy Environ. Sci.*, 2008, **1**, 66; (*c*) A. Mishra, M. K. R. Fischer and P. Bäuerle, *Angew. Chem., Int. Ed.*, 2009, **48**, 2474; (*d*) H. Imahori, T. Umeyama and S. Ito, *Acc. Chem. Res.*, DOI: 10.1021/ar900034t.

4 (*a*) M. K. Nazeeruddin, R. Humphry-Baker, D. L. Officer, W. M. Campbell, A. K. Burrell and M. Grätzel, *Langmuir*, 2004, **20**, 6514; (*b*) W. M. Campbell, A. K. Burrell, D. L. Officer and K. W. Jolley, *Coord. Chem. Rev.*, 2004, **248**, 1363; (*c*) Q. Wang, W. M. Campbell, E. E. Bonfantani, K. W. Jolley, D. L. Officer, P. J. Walsh, K. Gordon, R. Humphry-Baker, M. K. Nazeeruddin and M. Grätzel, *J. Phys. Chem. B*, 2005, **109**, 15397; (*d*) W. M. Campbell, K. W. Jolley, P. Wagner, K. Wagner, P. J. Walsh, K. C. Gordon, L. Schmidt-Mende, M. K. Nazeeruddin, Q. Wang, M. Grätzel and D. L. Officer, *J. Phys. Chem. C*, 2007, **111**, 11760; (*e*) J. Rochford, D. Chu, A. Hagfeldt and E. Galoppini, *J. Am. Chem. Soc.*, 2007, **129**, 4655; (*f*) S. Eu, S. Hayashi, T. Umeyama, A. Oguro, M. Kawasaki, N. Kadota, Y. Matano and H. Imahori, *J. Phys. Chem. C*, 2007, **111**, 3528; (*g*) S. Hayashi, Y. Matsubara, S. Eu, H. Hayashi, T. Umeyama, Y. Matano and H. Imahori, *Chem. Lett.*, 2008, **37**, 846; (*h*) S. Eu, S. Hayashi, T. Umeyama, Y. Matano, Y. Araki and H. Imahori, *J. Phys. Chem. C*, 2008, **112**, 4396; (*i*) S. Hayashi, M. Tanaka, H. Hayashi, S. Eu, T. Umeyama, Y. Matano, Y. Araki and H. Imahori, *J. Phys. Chem. C*, 2008, **112**, 15576; (*j*) J. K. Park, H. R. Lee, J. Chen, H. Shinokubo, A. Osuka and D. Kim, *J. Phys. Chem. C*, 2008, **112**, 16691.

5 (*a*) X. Yang, Z. Dai, A. Miura and N. Tamai, *Chem. Phys. Lett.*, 2001, **334**, 257; (*b*) L. Luo, C.-F. Lo, C.-Y. Lin, I.-J. Chang and E. W.-G. Diau, *J. Phys. Chem. B*, 2006, **110**, 410; (*c*) C.-F. Lo, L. Luo, E. W.-G. Diau, I.-J. Chang and C.-Y. Lin, *Chem. Commun.*, 2006, 1430.

6 (*a*) E. Galoppini, *Coord. Chem. Rev.*, 2004, **248**, 1283; (*b*) C.-Y. Lin, C.-F. Lo, L. Luo, H.-P. Lu, C.-S. Hung and E. W.-G. Diau, *J. Phys. Chem. C*, 2009, **113**, 755.

7 C.-W. Lee, H.-P. Lu, C.-M. Lan, Y.-L. Huang, Y.-R. Liang, W.-N. Yen, Y.-C. Liu, Y.-S. Lin, E. W.-G. Diau and C.-Y. Yeh, *Chem.–Eur. J.*, 2009, **15**, 1403.

8 (*a*) S. M. Zakeeruddin, M. K. Nazeeruddin, R. Humphry-Baker, P. Péchy, P. Quagliotto, C. Barolo, G. Viscardi and M. Grätzel, *Langmuir*, 2002, **18**, 952; (*b*) P. Wang, S. M. Zakeeruddin, J. E. Moser, Md. K. Nazeeruddin, T. Sekiguchi and M. Grätzel, *Nat. Mater.*, 2003, **2**, 402.

9 (*a*) S. Ito, P. Chen, P. Comte, M. K. Nazeeruddin, P. Liska, P. Péchy and M. Grätzel, *Progr. Photovolt.: Res. Appl.*, 2007, **15**, 603; (*b*) S. Ito, T. N. Murakami, P. Comte, P. Liska, C. Grätzel, M. K. Nazeeruddin and M. Grätzel, *Thin Solid Films*, 2008, **516**, 4613.

10 C.-C. Chen, H.-W. Chung, C.-H. Chen, H.-P. Lu, C.-M. Lan, S.-F. Chen, L. Luo, C.-S. Hung and E. W.-G. Diau, *J. Phys. Chem. C*, 2008, **112**, 19151.

11 R. J. Ellingson, J. B. Asbury, S. Ferrere, H. N. Ghosh, J. R. Sprague, T. Lian and A. J. Nozik, *J. Phys. Chem. B*, 1998, **102**, 6455.

12 The emission decays shown in Fig. 4 were well fitted on convolution of the multi-exponential decay functions ($\sum_i A_i \exp(-\frac{\tau_i}{t})$) with the laser pulse (a Gaussian function with FWHM $\sim$220 fs), which yielded time coefficients τ_i (relative amplitudes A_i) of **YD11–YD13** sensitized on both films indicated in each plot.

13 Electron injection from the electronically excited state of porphyrin into the conduction band of TiO_2 competes with other radiative or non-radiative relaxation channels. The electron-injection quantum yield (Φ_{inj}) defines the fraction of photons absorbed by the porphyrin that are converted into electrons in the conduction band of TiO_2, which is formulated as $\Phi_{inj} = \frac{k_{inj}}{k_{inj}+k_{agg}+k_{nr}+k_r} \cong (\tau^{-1}_{TiO_2} - \tau^{-1}_{Al_2O_3}) \cdot \tau_{TiO_2} = 1 - \frac{\tau_{TiO_2}}{\tau_{Al_2O_3}}$, in which k_{inj} and k_{agg} represent the non-radiative rate coefficients of electron injection and aggregate-induced energy transfer, respectively; k_r and k_{nr} denote radiative and other non-radiative (*e.g.*, intersystem crossing) rate coefficients, respectively.

14 (*a*) Y. Tachibana, J. E. Moser, M. Grätzel, D. R. Klug and J. R. Durrant, *J.Phys. Chem.*, 1996, **100**, 20056; (*b*) B. Wenger, M. Grätzel and J. E. Moser, *J. Am. Chem. Soc.*, 2005, **127**, 12150.

15 P. R. F. Barnes, A. Y. Anderson, S. E. Koops, J. R. Durrant and B. C. O'Regan, *J. Phys. Chem. C*, 2009, **113**, 1126.

16 (*a*) L. Schmidt-Mende, W. M. Campbell, Q. Wang, K. W. Jolley, D. L. Officer, M. K. Nazeeruddin and M. Grätzel, *ChemPhysChem*, 2005, **6**, 1253; (*b*) J.-H. Yum, P. Chen, M. Grätzel and M. K. Nazeeruddin, *ChemSusChem*, 2008, **1**, 699.

